



# A modeling methodology for car-following behaviors of automated vehicles: Trade-off between stability and mobility

Yuqin Zhang<sup>a,1</sup>, Ke Ma<sup>b,1,\*</sup>, Zhigang Xu<sup>a,\*</sup>, Hang Zhou<sup>c</sup>, Chengyuan Ma<sup>c</sup>, Xiaopeng Li<sup>c,\*</sup>

<sup>a</sup> School of Information Engineering, Chang'an University, Xi'an, Shaanxi 710064, PR China

<sup>b</sup> Intelligent Transportation Thrust, System Hub, The Hong Kong University of Science and Technology (Guangzhou), Guangzhou, Guangdong 511453, PR China

<sup>c</sup> Civil & Environmental Engineering Department, University of Wisconsin-Madison, Madison, WI 53706, USA



## ARTICLE INFO

### Keywords:

Automated vehicles  
Car following  
Response delay  
Stability  
Mobility  
Safety

## ABSTRACT

Empirical studies have indicated that automated vehicle (AV) automakers tend to prioritize mobility over stability in designing car-following (CF) models, which may raise safety concerns. A likely explanation for this issue is that hardware-induced response delays challenge the ability of the CF models, as designed by automakers, to maintain an equilibrium between stability and mobility. To address these concerns, this study proposes a modeling methodology for the CF model in AVs aimed at achieving a trade-off between stability and mobility. This methodology seeks to identify the optimal parameters that enhance mobility under stability constraints. First, the linear CF model is calibrated using data from 20 commercial AVs produced by multiple automakers, and the unique response delay values of the linear CF model for each AV are identified. Next, the parameter regions ensuring stability are derived theoretically based on the calibrated response delays for each AV. An optimal mobility objective function is constructed to minimize time headway and reaction time, with the boundaries of the stable parameter regions serving as constraints. It allows the selection of CF parameters that maximize mobility while remaining within the stable regions. This proposed modeling method is applied to all AVs, and the optimal parameters are tested in simulations. Simulation results demonstrate that the proposed optimal model effectively dampens oscillations, reduces safety risks, and maintains shorter spacing, thus achieving an ideal trade-off between stability and mobility for AVs.

## 1. Introduction

Traffic oscillation, a phenomenon frequently observed in congested traffic, is a macroscopic manifestation primarily caused by unstable car-following (CF) behaviors (Chen et al., 2012; Laval and Leclercq, 2010; Sun et al., 2020). These unstable CF behaviors are typically attributed to delayed response or unsystematic acceleration (Treiber and Kesting, 2013; Wang et al., 2024), resulting in negative impacts on key traffic performance metric, including mobility, stability, and safety. Consequently, researchers have focused on developing analytical tools to define and measure unstable CF behaviors, as well as further dampen traffic oscillations (Ma and Li,

\* Corresponding authors.

E-mail addresses: [kma62@wisc.edu](mailto:kma62@wisc.edu) (K. Ma), [xuzhigang@chd.edu.cn](mailto:xuzhigang@chd.edu.cn) (Z. Xu), [xli2485@wisc.edu](mailto:xli2485@wisc.edu) (X. Li).

<sup>1</sup> These authors contributed equally to this work.

2022; Tian et al., 2021; Zhang et al., 2023, 2022).

To study these CF behaviors, researchers have introduced the stability concept from the control theory into CF behavior studies (Feng et al., 2019; Treiber and Kesting, 2013). The stability concept is categorized into two types: local stability and string stability. Specifically, the local stability refers to the ability of a following vehicle's trajectory to stabilize over time to its equilibrium state (Robert et al., 1959), characterized by the trend speed and ideal headway, even when subjected to a small perturbation from its immediately preceding vehicle. To simplify the analysis, these CF processes are often approximated as linear time-invariant (LTI) systems. This implies that the system's output remains consistent over time in response to any inputs, and the system adheres to the principle of linear superposition when subjected to multiple input signals. Mathematically, this system can be described by ordinary differential equations (ODEs), which describe the relationship between functions and their derivatives. However, finding a theoretical solution for these ODEs is challenging. Thus, the Laplace transform is employed to convert the ODE from the time domain to the complex-valued frequency domain, enabling the derivation of a transfer function to obtain an arithmetic solution. The string stability describes the condition where perturbations from a preceding vehicle are not amplified as they propagate upstream through the platoon (Chandler et al., 1958). Based on the transfer function, the Fourier transform, a special case of the bilateral Laplace transform, is used to derive a complex function of frequency.

By leveraging these analytical tools, several studies have demonstrated that traffic flow consisting of human-driven vehicles (HVs) is unstable (Ma et al., 2025; Tadaki et al., 2013). Jiang et al. conducted a field experiment involving 51 vehicles, confirming that human driving behavior is a primary driver of traffic oscillations (Jiang et al., 2017). These oscillations lead to increased fuel consumption and emissions (Stern et al., 2018), pose potential safety risks, and reduce overall mobility (Davis, 2004). Consequently, dampening oscillations is significant. However, addressing human factors, such as sudden accelerations or decelerations caused by driver fatigue or distraction, remains a significant challenge (Wang et al., 2022).

A high hope that automated vehicles (AVs), with precise sensors and accurate actuators, can improve mobility (Davis, 2004; Jiang et al., 2025). Treiber and Helbing (2001) reported that a 10 % penetration rate of AVs can reduce travel time increases due to traffic congestion by >80 %. If the proportion reaches 20 %, almost all congestion is eliminated. Similarly, Li et al. (Li and Wagner, 2019) found that deploying >70 % of AVs can achieve average travel times close to free-flow conditions, even under severe traffic congestion.

However, empirical studies have revealed that the CF model for commercial AVs exhibits instability (Gunter et al., 2021). Bareket et al. (2003) conducted experiments on three AVs, demonstrating that the speed of the following AVs exhibited significant overshoot in response to speed changes of the preceding AV at frequencies typical of highway driving. Milanés and Shladover (2014) observed similar results, indicating that even under moderate speed changes, the CF model for multiple consecutive AVs failed to achieve string stability. Research suggests that one of the primary reasons for the instability of the CF model in commercial AVs is the delay caused by sensor detections, command calculation, and dynamic response (Milanés and Shladover, 2014). Milanés and Shladover (2014) further reported that the delay causes a smooth overshoot in each acceleration phase, based on tests involving four commercial AVs.

Research has demonstrated that the time headway of AVs, a critical indicator inversely proportional to mobility, impacts traffic stability (Li, 2022; Ma et al., 2022; Shi and Li, 2021; Zhong et al., 2025). Gunter et al. (2020), based on field experimental data, calibrated an optimal velocity model with different time headways. The results indicated that the shorter time headway amplifies oscillations to a higher magnitude, indicating an unstable state, whereas longer time headway effectively dampens oscillations, achieving stability. Additionally, Swaroop et al. (Swaroop and Rajagopal, 2001) highlighted that a smaller time headway increases road throughput. Hung et al. (2024) further investigated the implications of time headway, building on this premise. This indicates a trade-off between stability and mobility. Thus, it is essential to find an algorithm that ensures high mobility under stable constraints.

This study proposes a CF modeling methodology designed to identify optimal parameters that enhance mobility and safety under stability constraints. Specifically, it involves four steps: Step 1. Calibrate the linear CF model and identify the response delay of the CF model for 20 commercial AVs based on their trajectory data. Step 2. Derive the stability conditions for each commercial AV using their identified response delay. Step 3. Formulate the optimal mobility objective function for the CF model, incorporating constraints derived from the stability conditions. Step 4. Identify the optimized parameters of the CF model for each AV. Simulation results demonstrate that the proposed optimal model achieves a trade-off between stability and mobility. The main contributions of this paper can be summarized as follows:

1. The CF models are calibrated by empirical datasets comprising 20 commercial AVs. The unique response delay for each AV is quantified. These delays indicate the potential reasons for the unstable CF behavior of commercial AVs.
2. The theoretical stability of the CF model for each commercial AV is analyzed. The results reveal that none of the commercial AV exhibits stable CF behavior.
3. A CF modeling methodology is proposed to identify the optimal CF model that achieves a trade-off between stability and mobility. These optimal CF models are also restricted to the same delay with commercial AVs but show significant enhancement in stability and safety.
4. The dynamic range of the proposed optimal model is identified to clarify the operational boundaries and offer valuable insights for future efforts in collecting highly dynamic data and developing corresponding models.

## 2. Problem formulation

### 2.1. CF model

Before introducing the CF model, it is necessary to define some notations. Let  $\mathcal{I} := \{0, \dots, I\}$  represent the index set of AVs in a

platoon, where  $I \in \mathbb{Z}^+$  denotes the total number of following AVs in the platoon. Here,  $i = 0, i \in \mathcal{I}$ , refers to the leading AV. The set  $\mathcal{T}_i := \{t_{1_i}, t_{2_i}, \dots, t_{T_i}\}$  contains consecutive time-stamped data for AV  $i$ , where  $T_i$  is the number of sampling time stamps. Each pair of consecutive time points is separated by a customized unit time interval, denoted by  $\delta$ .

A general expression for the CF model can be written as:

$$\hat{a}_i(t) = f(\Delta p_i(t - \theta_i), v_i(t - \theta_i), \Delta v_i(t - \theta_i)), \forall i \in I \setminus \{0\}, t \in \mathcal{T}_i, \theta_i \in \mathcal{T}_i, t \geq \theta_i \quad (1)$$

where,  $\hat{a}_i(t)$  is the desired acceleration for the  $i$ th AV;  $\theta_i = n_i \delta$ , where  $n_i \in \mathbb{Z}^+$ , denotes the response delay of the  $i$ th AV;  $\Delta p_i(t) = p_i - p_{i-1}(t) - l$  is the gap between the  $i$ th AV and its predecessor,  $p_i(t)$  is the position of the  $i$ th AV at time  $t$ ,  $l$  is the length of AVs,  $l = 4.5m$ ;  $v_i(t)$  is the speed of the  $i$ th AV at time  $t$ ;  $\Delta v_i(t) = v_{i-1}(t) - v_i(t)$  is the relative speed between the  $i$ th AV and its predecessor; Note that  $\dot{p}_i(t) = v_i(t)$ ,  $\dot{v}_i(t) = a_i(t)$ . The function  $f(\cdot)$  refers to an arbitrary model, which is specifically linear as shown in Eq. (2).

$$\hat{a}_i(t) = f_i^{\Delta p} \Delta p_i(t - \theta_i) + f_i^v v_i(t - \theta_i) + f_i^{\Delta v} \Delta v_i(t - \theta_i) + z_i \quad (2)$$

where,  $f_i^{\Delta p} > 0$ ,  $f_i^v < 0$ , and  $f_i^{\Delta v} > 0$  are the gains of the corresponding factors.  $z_i$  refer to a model error for the  $i$ th AV, which is used to correct the CF model. It should be noted that AVs typically feature multiple selectable gear options. These gear options correspond to different time headways, denoted by  $T_d$ , where  $T_d = -f_i^v/f_i^{\Delta p}$ . The minimum gap of stopped AVs is  $\Delta p_i^0$ , where  $\Delta p_i^0 = -z_i/f_i^{\Delta p}$ .

## 2.2. Calibration of CF model

In this study, the calibration is based on the trajectories of 20 commercial AVs from the ULTRA-AV dataset (Zhou et al., 2024), which involves multiple CF data samples from different automakers. Before calibrating the CF model, it is necessary to preprocess the data by filtering out the stopped vehicles or those with near-zero speeds, as these states are challenging to represent within the model. In the ULTRA-AV dataset, the sampling interval is 0.1 s.

Based on the filtered data, the response delay  $\theta_i$  is calibrated. The calibration method can be expressed as:

$$\min GoF = F(MoP^{obs}, MoP^{sim}) \quad (3)$$

subject to :  $LB_{\rho_i} \leq \rho_i \leq UB_{\rho_i}$  where,  $\rho_i$  is the parameter matrix of the calibrated CF model,  $\rho_i = [f_i^{\Delta p} f_i^v f_i^{\Delta v} z_i \theta_i]$ .  $MoP^{sim}$  and  $MoP^{obs}$  are the simulated and observed measures of performance (MoPs), respectively.  $MoP^{sim}$  is obtained from the CF model simulation, as shown in Eq. (2). In this study, gap  $\Delta p_i(t)$ , speed  $v_i(t)$ , and acceleration  $a_i(t)$  are selected as MoPs.  $F(\cdot)$  is the goodness-of-fit function (GoF), which is utilized to quantify the error between the simulated trajectory and the observed trajectory. The objective of CF model calibration is to minimize the function. In this study,  $F(\cdot)$  is specified with the function of Normalized Root Mean Square Error (NRMSE), as shown in Eq. (4).  $LB_{\rho_i}$  and  $UB_{\rho_i}$  are the lower and upper bounds of the CF model parameter matrix. The genetic algorithm (GA) is employed to calibrate the model. Previous research by Punzo et al. (2021) has already shown that this combination performs excellently in calibrating various models and datasets.

$$GoF = \sum_{k=1}^3 \alpha_k \cdot NRMSE_{\{x_{i,k}\}} \quad (4)$$

where,  $NRMSE_{\{x_{i,k}\}} = \frac{\sqrt{\frac{1}{T} \sum_{t=1}^T \left[ x_{i,k}^{sim}(t) - x_{i,k}^{obs}(t) \right]^2}}{\sqrt{\frac{1}{T} \sum_{t=1}^T \left[ x_{i,k}^{obs}(t) \right]^2}}, k = 1, 2, 3$ . Let  $[x_{i,1}(t); x_{i,2}(t); x_{i,3}(t)] = [\Delta p_i(t); v_i(t); a_i(t)]$ .  $\alpha_k$  is the coefficient.  $x_{i,k}^{sim}(t)$  and  $x_{i,k}^{obs}(t)$  are the simulated and the observed MoP, respectively.

The calibration process consists of three main steps:

- Step 1: The first state of the data is used as the initial state for simulation. Within the predefined parameter range for the calibration model ( $0 < f_i^{\Delta p} < 0.2$ ,  $0 < f_i^v < 1$ ,  $-0.2 < f_i^v < 0$ ,  $-0.5 < z_i < 0.0$ ,  $0 < \theta_i < 2$ ), 100 sets of solutions are randomly selected (with a population size of 100 for the GA) as the initial model parameters.
- Step 2: These 100 sets of parameters are substituted into the model for simulation, and  $GoF$  is computed using Eq. (4).
- Step 3: Based on the results of Step 2, the GA updates the model parameters and repeats Step 2 until the stopping criterion for the GA is met (the maximum iteration is set to 1000). The model parameters corresponding to the minimum  $GoF$  are then output as the final solution.

Based on the calibration process described above, further statistical analysis is conducted. In the ULTRA-AV dataset, multiple trajectories exist for each AV, and each trajectory corresponds to a specific response delay. Fig. 1 presents the statistical results of all response delays for four selected AVs in the dataset, specifically Audi (A6), BMW (X5), Mercedes (A-Class), and Tesla (Model 3). These four AVs are used as cases in subsequent analyses. In Fig. 1, each colored violin-shaped plot represents the response delay distribution of the CF model for a specific commercial AV. The boxplot within each violin plot provides additional statistical insights. The upper boundary of the rectangle represents the third quartile (Q3) of the data, indicating that 75 % of the data points are at or below this

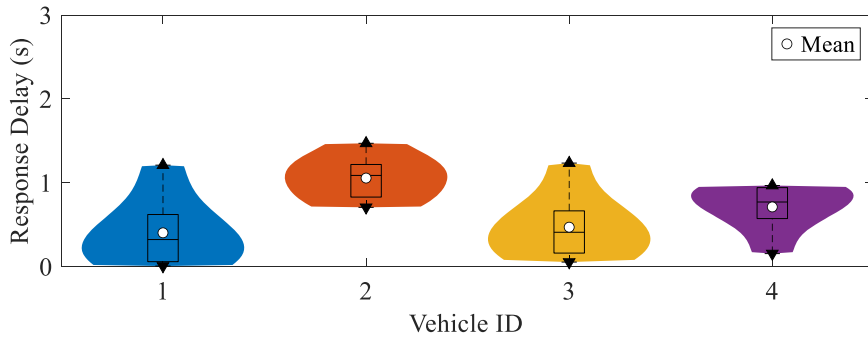


**Fig. 1.** Statistical results of response delay for the four selected AVs.

**Table 1**

The calibration parameters for the four selected AVs.

AV ID	$f_i^{\Delta v} (s^{-1})$	$f_i^{\Delta p} (s^{-2})$	$f_i^v (s^{-1})$	$T_d(s)$	$z_i(m/s^2)$	$\theta_i(s)$	$\min GoF$	$\Delta p_i^0 (m)$
1	0.3091	0.0876	-0.0984	1.1233	-0.1865	0.3479	0.2492	2.1290
2	0.1666	0.0684	-0.1622	2.3714	-0.1618	1.0291	0.0885	2.3655
3	0.346	0.0751	-0.0775	1.0320	-0.2091	0.4605	0.1527	2.7843
4	0.4225	0.1757	-0.1814	1.0324	-0.5	0.7059	0.1096	2.8458

value. Similarly, the bottom boundary of the rectangle represents the first quartile (Q1) of the data. It shows that 25 % of the data points are at or below this value. The middle line of the box represents the median of the data. The median divides the dataset into two equal parts, with half of the data points lying above it and the other half below. The upper and lower black triangles represent the maximum and minimum values of the data, excluding any outliers. The white dots indicate the mean response delay of the CF model for each AV.

[Table 1](#) presents the calibration results of the CF model for the four selected AVs. As mentioned above, each AV has multiple trajectories, so the results shown in [Table 1](#) correspond to the response delay of the CF model for the trajectory whose value is closest to the mean. Additionally, we calibrated the CF models for 16 other commercial AVs from the ULTRA-AV dataset, as detailed in [Table A.1](#) in the Appendix. The results reveal that the response delays of the CF model for 20 commercial AVs range from 0.4 to 1.1 s, with the majority of the delays concentrated between 0.5 and 0.8 s.

### 3. Stability analyses

Before deriving the stability constraints, it is necessary to obtain the transfer function of the CF model. The transfer function can be derived by taking the derivative of both sides of the [Eq. \(2\)](#) and applying the Laplace transformation. The resulting transfer function is given by:

$$H_i(s) = \frac{V_i(s)}{V_{i-1}(s)} = \frac{f_i^{\Delta v} s e^{-\theta_i s} + f_i^{\Delta p} e^{-\theta_i s}}{s^2 + (f_i^{\Delta v} - f_i^v) s e^{-\theta_i s} + f_i^{\Delta p} e^{-\theta_i s}}, \quad s \in \mathbb{C} \quad (5)$$

where,  $V_i(s) = \int_0^\infty v_i(t) e^{-st} dt$  is the Laplace transform of output  $v_i(t)$ ,  $V_{i-1}(s) = \int_0^\infty v_{i-1}(t) e^{-st} dt$  is the Laplace transform of input  $v_{i-1}(t)$ .  $s$  represents a complex number in the Laplace transform, and  $\mathbb{C}$  is the set of complex numbers.

#### 3.1. Local stability

A platoon that is locally stable implies that disturbances of the AVs converge to the equilibrium point while the preceding AV travels at a constant speed. To ensure local stability, the closed-loop system must have eigenvalues with strictly negative real parts ([Zhou et al., 2019a](#)). The sufficient condition for this is provided by the Routh-Hurwitz Criterion. However, it should be noted that the  $H_i(s)$  in [Eq. \(5\)](#) is an irrational fraction, making direct stability analysis challenging using conventional methods. To address this, the first-order Padé approximation is employed to transform this irrational fraction into a rational one.

Let  $F(s) = e^{\theta_i s}$ ,  $R(s) = \frac{a_0 + a_1 s}{1 + b_1 s}$ , so the following equation holds:

$$F(s)|_{s=0} = 1, R(s)|_{s=0} = a_0$$

$$F'(s)|_{s=0} = \theta_i e^{\theta_i s}|_{s=0} = \theta_i, R'(s)|_{s=0} = \frac{a_1(1+b_1s) - (a_0+a_1s)b_1}{(1+b_1s)^2}|_{s=0} = a_1 - b_1$$

$$F''(s)|_{s=0} = \theta_i^2 e^{\theta_i s}|_{s=0} = \theta_i^2,$$

$$R''(s)|_{s=0} = \frac{-2b_1(a_1(1+b_1s) - (a_0+a_1s)b_1)(1+b_1s)}{(1+b_1s)^4}|_{s=0} = -2b_1(a_1 - b_1)$$

According to Padé approximation, the following equation holds:

$$\left\{ \begin{array}{l} a_0 = 1 \\ a_1 - b_1 = \theta_i \\ -2b_1(a_1 - b_1) = \theta_i^2 \end{array} \right. \xrightarrow{\text{yields}} \left\{ \begin{array}{l} a_0 = 1 \\ a_1 = \frac{1}{2}\theta_i \\ b_1 = -\frac{1}{2}\theta_i \end{array} \right. \quad (6)$$

Therefore, for  $\forall i \in \mathcal{I} \setminus \{0\}$ ,  $s \in \mathbb{C}$ , the following equation satisfies:

$$e^{\theta_i s} \approx \frac{2 + \theta_i s}{2 - \theta_i s} \quad (7)$$

Thus, the transfer function can be rewritten as:

$$\begin{aligned} H_i(s) &= \frac{f_i^{\Delta v}s + f_i^{\Delta p}}{e^{\theta_i s}s^2 + (f_i^{\Delta v} - f_i^v)s + f_i^{\Delta p}} \\ &\approx \frac{-f_i^{\Delta v}\theta_i s^2 + (2f_i^{\Delta v} - f_i^{\Delta p})\theta_i s + 2f_i^{\Delta p}}{\theta_i s^3 + [2 - (f_i^{\Delta v} - f_i^v)\theta_i]s^2 + [2(f_i^{\Delta v} - f_i^v) - f_i^{\Delta p}\theta_i]s + 2f_i^{\Delta p}} \end{aligned} \quad (8)$$

Hence, the characteristic equation of the system is obtained:  $P(s) = \theta_i s^3 + [2 - (f_i^{\Delta v} - f_i^v)\theta_i]s^2 + [2(f_i^{\Delta v} - f_i^v) - f_i^{\Delta p}\theta_i]s + 2f_i^{\Delta p}$ . According to the Routh-Hurwitz criterion, for a third-order polynomial,  $P(s) = A_3 s^3 + A_2 s^2 + A_1 s + A_0$ , the closed-loop system is local stable if and only if:  $A_n > 0$  and  $A_2 A_1 > A_3 A_0$ ,  $n \in \{0, 1, 2, 3\}$ . Since  $\theta_i > 0$  and  $f_i^{\Delta p} > 0$  are established in Section 2.1, it suffices to ensure that the following expression holds:

$$A_2 \underline{\underline{def}} 2 - (f_i^{\Delta v} - f_i^v)\theta_i > 0 \quad (9)$$

$$A_1 \underline{\underline{def}} 2(f_i^{\Delta v} - f_i^v) - f_i^{\Delta p}\theta_i > 0 \quad (10)$$

$$A_4 \underline{\underline{def}} [2 - (f_i^{\Delta v} - f_i^v)\theta_i][2(f_i^{\Delta v} - f_i^v) - f_i^{\Delta p}\theta_i] - 2f_i^{\Delta p}\theta_i > 0 \quad (11)$$

### 3.2. String stability

String stability is defined as the oscillation from the preceding AV being strictly dampening in each CF pair (Sun et al., 2018; Treiber and Kesting, 2013; Zhou et al., 2019b), which can be mathematically expressed as:

$$\|\varepsilon_I\|_\infty < \dots < \|\varepsilon_i\|_\infty < \dots < \|\varepsilon_1\|_\infty < \|\varepsilon_0\|_\infty \quad (12)$$

where,  $\|\varepsilon_i\|_\infty = \sup_t |\varepsilon_i(t)|$  is the least upper bound of oscillation's absolute value for the AV  $i$ . The string is considered stable for  $\|\varepsilon_i(t)\|_\infty < \|\varepsilon_{i-1}(t)\|_\infty$  when  $|H_i(j\omega)| < 1$  (Sun et al., 2018; Zhou et al., 2023). Here,  $j$  denotes the imaginary unit, defined as  $j = \sqrt{-1}$ , and  $\omega$  represents the angular frequency, measured in radians per second (rad/s).

Proof:

Let  $\varepsilon_{i-1}(t) = e^{st} = e^{j\omega t}$  be a general periodic input to the system  $H_i(j\omega)$ . For this input, the output of this system will be a non-sinusoidal periodic function, which can be expressed in terms of a Fourier series as:

$$\varepsilon_i(t) = \sum_{k=0}^{\infty} \alpha_k \cos(k\omega t) + \beta_k \sin(k\omega t) \quad (13)$$

Since the transfer function has low-pass characteristics, it can be assumed to a good degree of approximation that all higher harmonics of  $\varepsilon_i(t)$  are filtered out during the process, mainly contributed by the fundamental harmonics. Thus, we assume that only the fundamental harmonic component of the output. Since the higher harmonics in the output are often of smaller amplitude than the amplitude of the fundamental harmonic component. Therefore,

$$\varepsilon_i(t) \approx \alpha_1 \cos(\omega t) + \beta_1 \sin(\omega t) \quad (14)$$

where,  $\alpha_1$  and  $\beta_1$  are the imaginary and real parts of the transfer function, respectively. They can be expressed as:

$$\begin{cases} \alpha_1 = \frac{1}{\pi} \int_0^{2\pi} \varepsilon_i(t) \cos(\omega t) d(\omega t) \\ \beta_1 = \frac{1}{\pi} \int_0^{2\pi} \varepsilon_i(t) \sin(\omega t) d(\omega t) \end{cases} \quad (15)$$

In the frequency domain, the transfer function  $H_i(j\omega)$  can be represented as a phasor and frequency function:

$$M_i \angle \phi_i = \beta_1 + j\alpha_1 = \sqrt{\beta_1^2 + \alpha_1^2} \angle \arctan\left(\frac{\alpha_1}{\beta_1}\right) \quad (16)$$

Thus, the output expression for  $\varepsilon_i(t)$  is

$$\varepsilon_i(t) = H_i(j\omega) e^{j\omega t} = M_i e^{j(\omega t + \phi_i)} = M_i \cos(\omega t + \phi_i) + j M_i \sin(\omega t + \phi_i) \quad (17)$$

where  $M_i = \sqrt{\beta_1^2 + \alpha_1^2} = |H_i(j\omega)|$  and  $\phi_i = \arctan\frac{\alpha_1}{\beta_1} = \arctan H_i(j\omega)$  represent the amplitude gain and phase offset of the transfer function. The string is stable if  $\|\varepsilon_i(t)\|_\infty < \|\varepsilon_{i-1}(t)\|_\infty$ , for  $\forall i \in \mathcal{I} \setminus \{0\}$ , which holds when  $M_i = |H_i(j\omega)| < 1$ .

Q.E.D.

Due to the presence of the exponential term in Eq. (5), Euler's formula is introduced, and  $H_i(s)$  in Eq. (5) is rewritten by substituting  $s = j\omega$  for  $\forall i \in \mathcal{I} \setminus \{0\}, \omega \in R^+$ .

$$H_i(j\omega) = \frac{f_i^{\Delta v} \omega j + f_i^{\Delta p}}{[f_i^{\Delta p} - \omega^2 \cos(\theta_i \omega)] + j[(f_i^{\Delta v} - f_i^v) \omega - \omega^2 \sin(\theta_i \omega)]} \quad (18)$$

To satisfy  $|H_i(j\omega)| < 1$ , i.e.,  $|H_i(j\omega)|^2 < 1$ , the following inequality must hold:

$$|H_i(j\omega)|^2 = \frac{(f_i^{\Delta v} \omega)^2 + f_i^{\Delta p 2}}{(f_i^{\Delta p} - \omega^2 \cos(\theta_i \omega))^2 + ((f_i^{\Delta v} - f_i^v) \omega - \omega^2 \sin(\theta_i \omega))^2} < 1 \quad (19)$$

The above expression can be further rewritten as

$$\omega^2 - 2(f_i^{\Delta v} - f_i^v) \sin(\theta_i \omega) \omega + [(f_i^{\Delta v} - f_i^v)^2 - 2f_i^{\Delta p} \cos(\theta_i \omega) - f_i^{\Delta v 2}] > 0 \quad (20)$$

To simplify the above inequality, the sine and cosine terms are expanded using the Taylor series:

$$\begin{cases} \sin(\theta_i \omega) = \theta_i \omega - \frac{1}{6}(\theta_i \omega)^3 + o(\theta_i \omega) \\ \cos(\theta_i \omega) = 1 - \frac{1}{2}(\theta_i \omega)^2 + o(\theta_i \omega) \end{cases} \quad (21)$$

Substituting Eq. (21) into Eq. (20) yields:

$$\begin{aligned} \omega^2 - 2(f_i^{\Delta v} - f_i^v) \left[ \theta_i \omega - \frac{1}{6}(\theta_i \omega)^3 \right] \omega + [(f_i^{\Delta v} - f_i^v)^2 - 2f_i^{\Delta p} \left[ 1 - \frac{1}{2}(\theta_i \omega)^2 \right] - f_i^{\Delta v 2}] \\ = \frac{1}{3} (f_i^{\Delta v} - f_i^v) \theta_i^3 \omega^4 + [1 - 2(f_i^{\Delta v} - f_i^v) \theta_i + f_i^{\Delta p} \theta_i^2] \omega^2 + (f_i^{\Delta v} - f_i^v)^2 - 2f_i^{\Delta p} - f_i^{\Delta v 2} > 0 \end{aligned} \quad (22)$$

It is a quadratic equation in terms of  $\omega^2$ . For convenience in subsequent analysis, the following definitions are introduced:

$$\begin{cases} A \underset{3}{\underline{\underline{def}}} (f_i^{\Delta v} - f_i^v) \theta_i^3 \\ B \underset{1}{\underline{\underline{def}}} 1 - 2(f_i^{\Delta v} - f_i^v) \theta_i + f_i^{\Delta p} \theta_i^2 \\ C \underset{2}{\underline{\underline{def}}} (f_i^{\Delta v} - f_i^v)^2 - 2f_i^{\Delta p} - f_i^{\Delta v 2} \end{cases} \quad (23)$$

Therefore, the following expression can be derived:

**Table 2**

Stable parameters of CF model for the four selected AVs.

Parameter	AV 1	AV 2	AV 3	AV 4
$f_i^{\Delta v}(s^{-1})$	0.0120	0.0040	0.0421	0.0261
$f_i^{\Delta p}(s^{-2})$	0.0661	0.0301	0.0361	0.0461
$f_i^v(s^{-1})$	-0.4529	-0.3146	-0.2665	-0.3427
$T_d(s)$	6.8517	10.4518	7.3823	7.4338

$$B^2 - 4AC = f_i^{\Delta p^2} \theta_i^4 + \left[ -\frac{4}{3}(f_i^{\Delta v} - f_i^v)f_i^{\Delta p} + \frac{8}{3}f_i^{\Delta v^2}f_i^v - 4f_i^{v^2}f_i^{\Delta v} + \frac{4}{3}f_i^{v^3} \right] \theta_i^3 + \\ 2 \left[ 2(f_i^{\Delta v} - f_i^v)^2 + f_i^{\Delta p} \right] \theta_i^2 - 4(f_i^{\Delta v} - f_i^v)\theta_i + 1 \quad (24)$$

From Eq. (2), it is evident that  $f_i^v < 0$ , which implies  $A > 0$ . To ensure the validity of Eq. (22), it is necessary to analyze different cases based on the sign of  $B$ .

- Case 1: For  $B > 0$ , the condition  $C > 0$  must be satisfied to ensure the validity of Eq. (22).
- Case 2: For  $B < 0$ , the condition  $B^2 - 4AC < 0$  must be met to guarantee that the Eq. (22) holds.

Thus, two stable regions can be derived, whose expressions are as follows:

Stable region 1:  $B > 0$ ,  $C > 0$ ,  $A_4 > 0$ ,  $A_1 > 0$ , and  $A_2 > 0$ ;

Stable region 2:  $B < 0$ ,  $B^2 - 4AC < 0$ ,  $A_4 > 0$ ,  $A_1 > 0$ , and  $A_2 > 0$ ;

To more clearly illustrate the trade-off between stability and mobility achieved by the optimal CF model proposed in this paper, the stable parameters of the CF model for the four selected AVs are provided in Table 2. The stable parameters of the CF model are randomly selected within the stable region, which helps mitigate potential biases that might arise from focusing exclusively on specific points, thereby enhancing the comprehensiveness and reliability of the experimental results. The results demonstrate that the time headway can reach up to an average of 6.2 times that of the calibrated result, indicating a significant sacrifice in mobility while ensuring stability. Therefore, the next section will focus on constructing an optimal mobility objective function and identifying the best model parameters that ensure higher mobility and under stability constraints.

#### 4. Modeling methodology

Consider a CF pair where the CF model is stable before  $t = 0$ , i.e.,  $\Delta v(t) = 0$ ,  $a_i(t) = a_{i-1}(t) = 0$ ,  $\forall t < 0$ . At  $t = 0$ , the preceding AV experiences an acceleration  $a_{i-1} > 0$ . Since the existence of a response delay, denoted by  $\theta_i$ , the following AV must achieve an acceleration equal to  $a_{i-1}$  (or larger than  $a_{i-1}$ ) before reaching a stable state. Let  $t^*$  denote the time required for the following AV to reach the acceleration  $a_{i-1}$ , referred to as the reaction time. At time  $\theta_i + t^*$ ,  $a_i(\theta_i + t^*) = a_{i-1}$ , and  $a_i(t) < a_{i-1}$ ,  $\forall t \in (0, t^*]$ .

The dynamics of the following AV can be described as:

$$a_i(\theta_i + t) = f_i^{\Delta v} \Delta v_i(t) + f_i^{\Delta p} \Delta p_i(t) + f_i^v v_i(t) + z_i \quad (25)$$

At  $t = 0$ , the initial condition is:

$$a_i(\theta_i) = f_i^{\Delta p} \Delta p_i(0) + f_i^v v_i(0) + z_i = 0 \quad (26)$$

Subtracting Eq. (26) from Eq. (25) yields:

$$a_i(\theta_i + t) = f_i^{\Delta v} \Delta v_i(t) + f_i^{\Delta p} (\Delta p_i(t) - \Delta p_i(0)) + f_i^v (v_i(t) - v_i(0)) \quad (27)$$

During the time interval  $t \in (0, t^*]$ , the following AV has an acceleration smaller than  $a_{i-1}$ . Therefore, the following inequalities hold:

$$\Delta p_i(t^*) - \Delta p_i(0) \leq \frac{1}{2} a_{i-1} t^{*2} \quad (28)$$

$$\Delta v_i(t^*) \leq a_{i-1} t^* \quad (29)$$

$$v_i(t^*) - v_i(0) \geq 0 \quad (30)$$

Combining Eq. (27) to Eq. (30), we obtain:

$$a_i(\theta_i + t^*) - a_{i-1} \leq \frac{1}{2} a_{i-1} t^{*2} f_i^{\Delta p} + f_i^{\Delta v} a_{i-1} t^* - a_{i-1} \quad (31)$$

Since  $a_i(\theta_i + t^*) = a_{i-1}$ , the following condition must be satisfied:

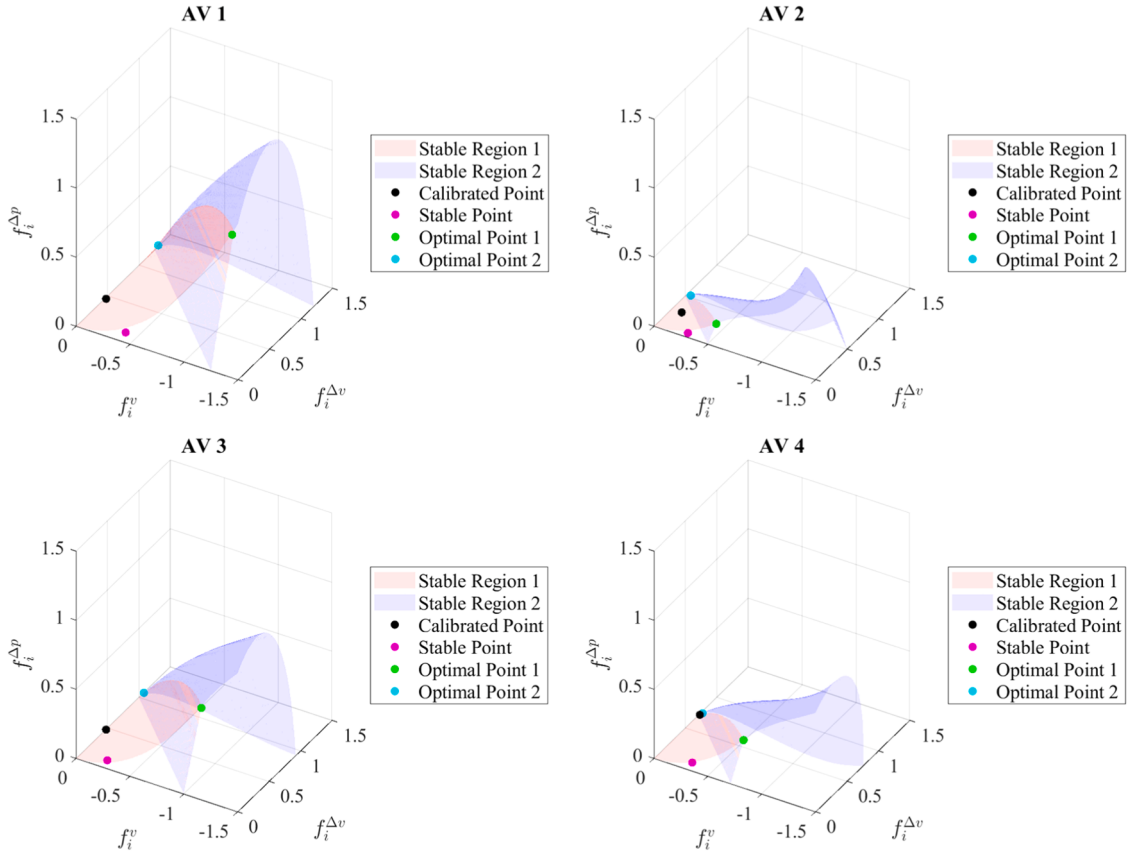


**Fig. 2.** The relationship between four sets of parameters and their corresponding stable regions.

$$\frac{1}{2}t^{*2}f_i^{\Delta p} + f_i^{\Delta v}t^* - 1 \geq 0 \quad (32)$$

Thus, the lower bound of the time for the following AV to reach the target acceleration is

$$T_i^e = \frac{-f_i^{\Delta v} + \sqrt{(f_i^{\Delta v})^2 + 2f_i^{\Delta p}}}{f_i^{\Delta p}} \quad (33)$$

The results can also be extended to the case where \$a\_{i-1} < 0\$, where \$T\_i^e\$ is the upper bound of the reaction time for the following AV to reach \$a\_{i-1}\$. These results remain valid in the scenario where the CF model enters stable states, i.e., initially, the two AVs accelerate or decelerate at a certain rate, and then the preceding AV maintains a constant speed. In the optimization problem, \$T\_i^e\$ is used to quantify the efficiency of the AV in reaching the target acceleration.

For each AV, the optimization objective function is defined in Eq. (34). The constraints are derived from the stability regions obtained in Section 3. The stability regions for each AV, along with the corresponding model parameters, are collectively illustrated in Fig. 2 at the end of this section.

$$\text{Min } f_i = w_1 T_d + w_2 T_i^e \quad (34)$$

$$\text{s.t. } \{f_i^{\Delta v}, f_i^{\Delta p}, T_d\} \in (R_1 \cup R_2) \cap R_3 \quad (35)$$

$$0 < f_i^{\Delta v} < 1.5 \quad (36)$$

$$0 < f_i^{\Delta p} < 1.5 \quad (37)$$

$$0 < T_d < 5 \quad (38)$$

where,

**Table 3**

The optimal parameters in stable region 1 and stable region 2.

Parameter	Stable Region1				Stable Region2			
	AV 1	AV 2	AV 3	AV 4	AV 1	AV 2	AV 3	AV 4
$f_i^{\Delta v}(s^{-1})$	0.001	0.001	0.001	0.001	1.2296	0.4667	0.9767	0.6863
$f_i^{\Delta p}(s^{-2})$	1.0333	0.1662	0.6633	0.3455	0.0548	0.0346	0.0589	0.0367
$f_i'(s^{-1})$	-1.4461	-0.5795	-1.1633	-0.8324	-0.0442	-0.0715	-0.0604	-0.0522
$T_d(s)$	1.3995	3.4872	1.7538	2.4093	0.8068	2.0702	1.0257	1.4228
$\min(f_i(s))$	1.3949	3.4752	1.7443	2.4063	0.8029	1.9954	1.0099	1.4136

$$R_1 = \begin{cases} 1 - 2(f_i^{\Delta v} + f_i^{\Delta p} T_d) \theta_i + f_i^{\Delta p} \theta_i^2 > 0 \\ f_i^{\Delta p} (T_d)^2 - 2f_i^{\Delta v} T_d - 2 > 0 \end{cases} \quad (39)$$

$$R_2 = \begin{cases} 1 - 2(f_i^{\Delta v} + f_i^{\Delta p} T_d) \theta_i + f_i^{\Delta p} \theta_i^2 < 0 \\ \frac{4}{3}(-f_i^{\Delta p} \theta_i)^3 T_d^3 + [4(-f_i^{\Delta p} \theta_i)^2 - 4(-f_i^{\Delta p})^2 f_i^{\Delta v} \theta_i^3] T_d^2 \\ + \left( -4f_i^{\Delta p} \theta_i + 8f_i^{\Delta v} f_i^{\Delta p} \theta_i^2 - \frac{8}{3}f_i^{\Delta v}^2 f_i^{\Delta p} \theta_i^3 - \frac{4}{3}(f_i^{\Delta p})^2 \theta_i^3 \right) T_d \\ + f_i^{\Delta p} \theta_i^4 - \frac{4}{3}f_i^{\Delta v} f_i^{\Delta p} \theta_i^3 + 2[2(f_i^{\Delta v})^2 + f_i^{\Delta p}] \theta_i^2 - 4f_i^{\Delta v} \theta_i + 1 < 0 \end{cases} \quad (40)$$

$$R_3 = \begin{cases} 2 - (f_i^{\Delta v} + f_i^{\Delta p} T_d) \theta_i > 0 \\ 2(f_i^{\Delta v} + f_i^{\Delta p} T_d) - f_i^{\Delta p} \theta_i > 0 \\ [2 - (f_i^{\Delta v} + f_i^{\Delta p} T_d) \theta_i][2(f_i^{\Delta v} + f_i^{\Delta p} T_d) - f_i^{\Delta p} \theta_i] - 2f_i^{\Delta p} \theta_i > 0 \end{cases} \quad (41)$$

In this section, the GA is selected to find the optimal parameters within stable region 1 ( $R_1 \cap R_3$ ) and stable region 2 ( $R_2 \cap R_3$ ), respectively. The GA is particularly suitable for solving non-linear and multi-constrained optimization problems like the one presented in our study. The population size of GA is set to 1000 to balance computational efficiency and solution quality. The algorithm terminates when the change in population fitness is less than  $10^{-16}$  or reaches a predefined maximum number of iterations, which is 100 in this work. Setting  $w_1 = w_2 = 0.5$ . It is worth emphasizing that due to the introduction of approximation methods such as Padé approximation and Taylor series in deriving the stability constraints, there is a possibility that the final optimal solution may be unstable. In this case, when the solution in Eq. (12) is not satisfied, the solution will be discarded and re-optimized. The optimal parameters of the linear CF model for the four selected AVs are presented in Table 3, while those for 20 AVs are provided in Table A.2 of the Appendix. Since the optimal parameters are solely related to the response delay of the CF model and are independent of the specific AV, Table A.2 only includes the optimal parameters corresponding to different response delays of the CF models.

Fig. 2 demonstrates the relationship between four sets of parameters and the two stable regions of the CF model for each AV. In Fig. 2, the pink and purple areas represent stable region 1 ( $R_1 \cap R_3$ ) and stable region 2 ( $R_2 \cap R_3$ ), respectively. The calibrated point and the stable point correspond to the linear CF model parameters ( $f_i^{\Delta v}, f_i^{\Delta p}, f_i'$ ) derived from real data calibration and stability verification, respectively. The optimal point 1 and point 2 denote the optimal linear model parameters identified within stable region 1 and stable region 2, respectively, based on the designed objective function.

It can be demonstrated that all the calibrated points lie outside the stable regions, indicating that the calibrated models (CMs) for the four commercial AVs exhibit instability. More generally, the stability of the CM for 20 AVs in the ULtra-AV dataset is evaluated, as shown in Table A.1 in the Appendix. The results reveal that the CMs for all AVs are unstable. Furthermore, it is noteworthy that the optimal points 1 and 2 tend to lie near the boundaries of their respective stable region, with the optimal point 2 consistently being the point closest to the calibrated point. This suggests that the CF models for commercial AVs prioritize higher mobility but fail to achieve stability.

## 5. Performance testing

In this section, we conduct numerical simulations to evaluate the performances of the CM (CF model with the calibrated point), the stable model (SM, CF model with the stable point), the optimal model derived from stable region 1 (OM1, CF model with the optimal point 1), and the optimal model derived from stable region 2 (OM2, CF model with the optimal point 2). The simulation tests are designed to address the following questions:

- **EQ1:** Are the CMs for commercial AVs indeed unstable, as depicted in Fig. 2?

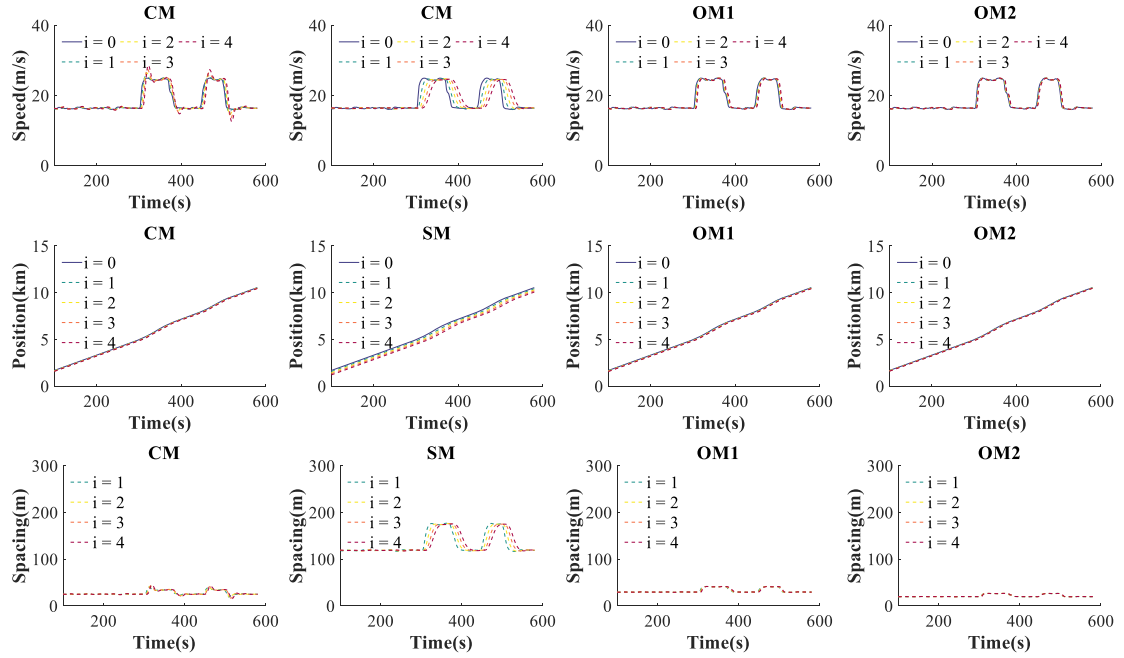


**Fig. 3.** The performances of the following AVs based on the four models for AV 1.

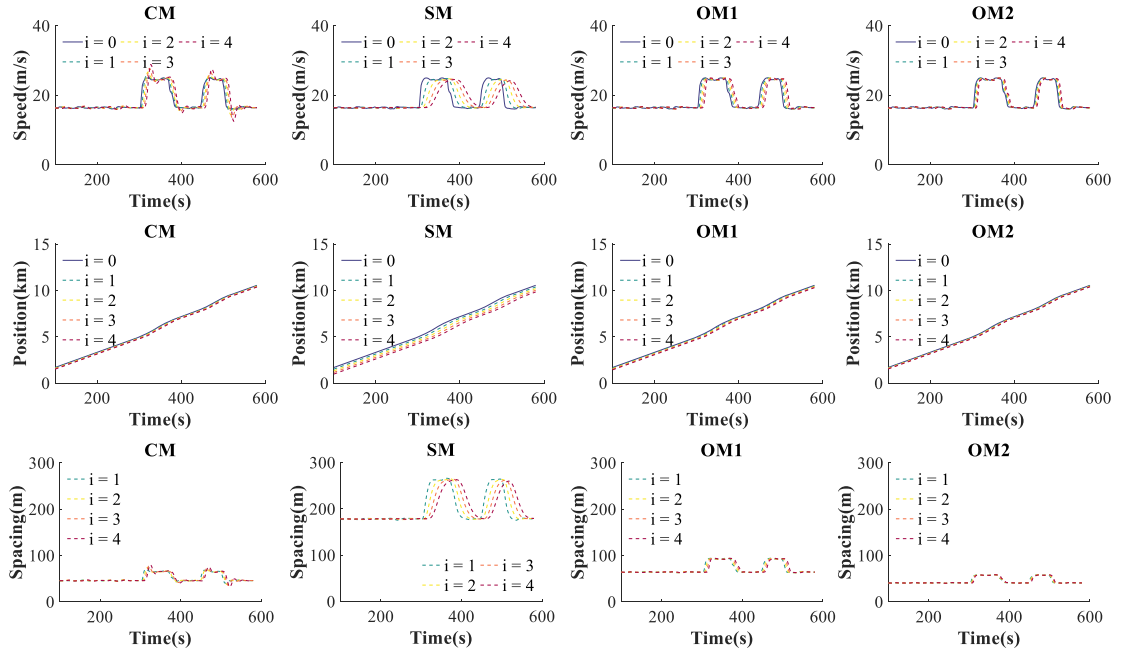


**Fig. 4.** The performances of the following AVs based on the four models for AV 2.

- **EQ2:** Do the optimal models achieve a trade-off between stability and mobility compared to the CMs and the SMs? How do they perform in terms of safety?
- **EQ3:** Which model performs better: OM1 or OM2?

Four models for each AV, namely CM, SM, OM1, and OM2, are tested based on a real trajectory. Figs. 3, 4, 5, 6 illustrate the stability and mobility of the four CF models for each selected AV, as assessed through their speed, position, and spacing performances. Each figure corresponds to one of these performance metrics of the following AVs ( $i = 1, 2, 3, 4$ ) based on the specific CF model.

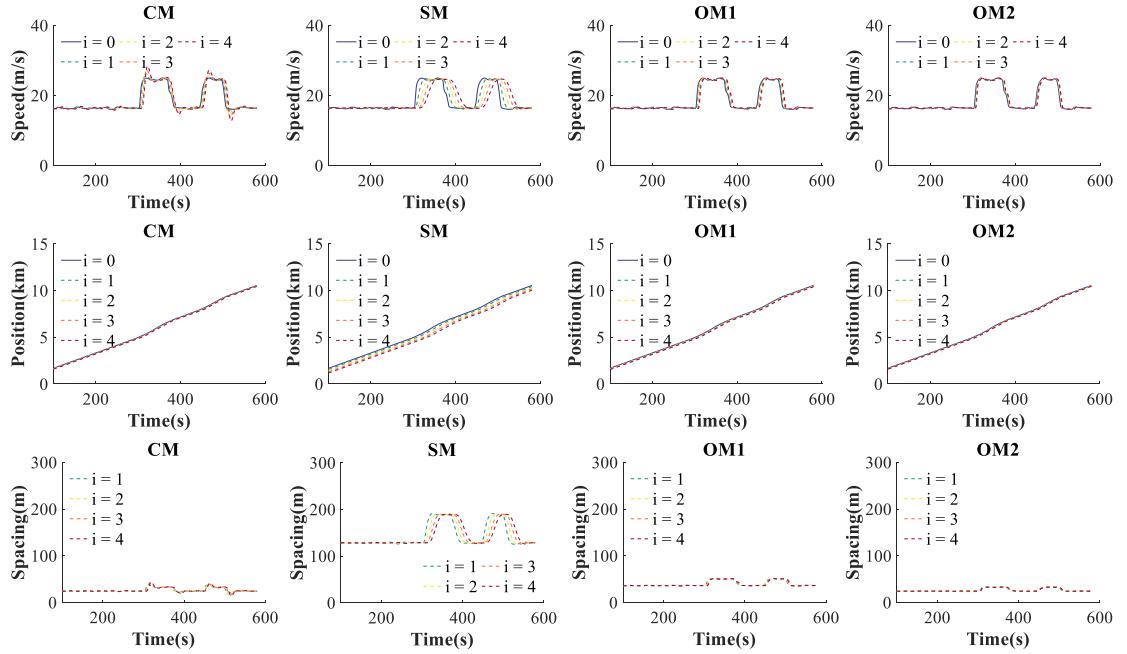


**Fig. 5.** The performances of the following AVs based on the four models for AV 3.

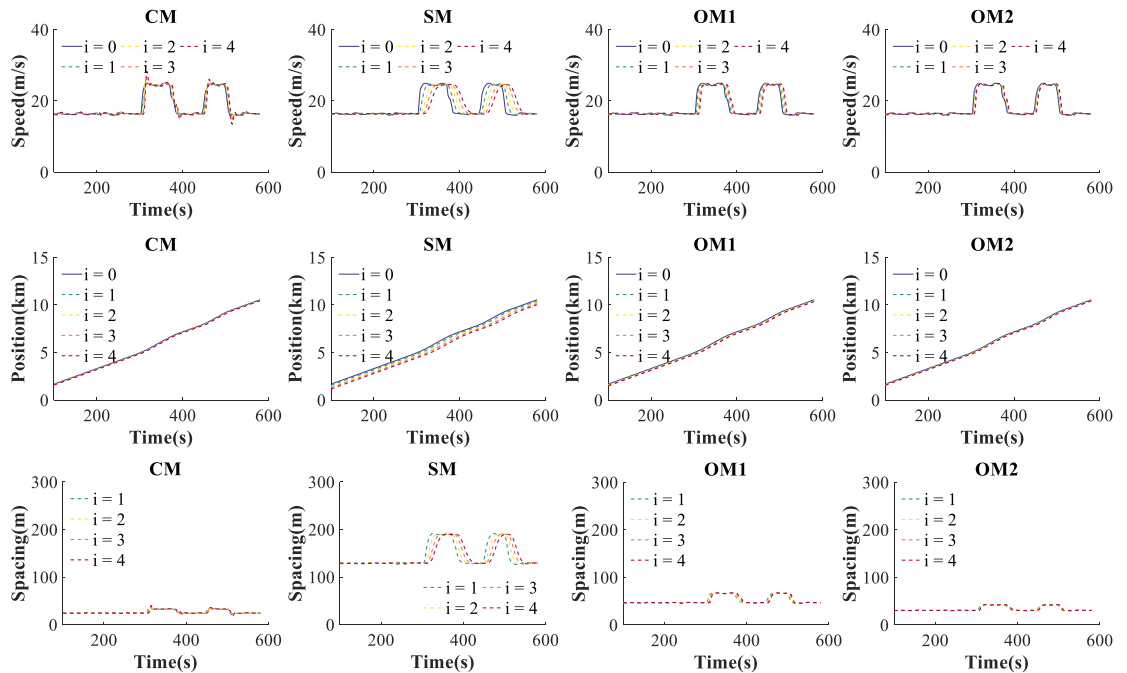


**Fig. 6.** The performances of the following AVs based on the four models for AV 4.

For EQ1, the results demonstrate that the speed performance of CMs exhibits significant overshoot, as shown in Figs. 3–6. In comparison, the speed performance of the other three models exhibits effective damping of oscillations. This confirms that all the CMs for commercial AVs are indeed unstable.

For EQ2 and EQ3, the standard deviation (SD) of speed, the average spacing, and the minimum time-to-collision (TTC) are statistically analyzed, as illustrated in Fig. 7. A lower speed SD indicates greater platoon stability, a shorter spacing reflects improved mobility, and a larger minimum TTC implies enhanced safety performance. The mathematical formulations for the speed SD, average

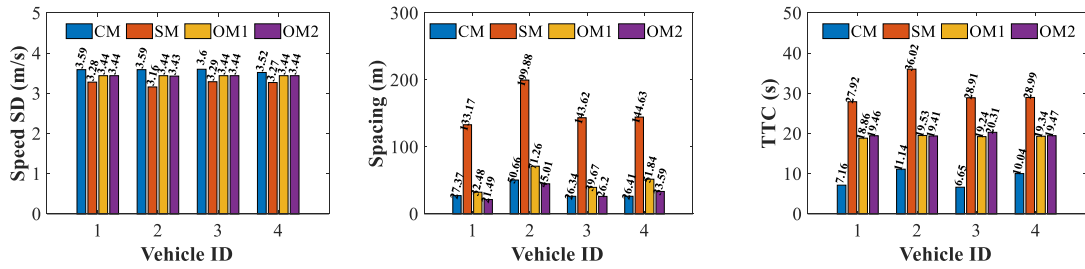


Fig. 7. The statistical results of the speed SD, the average spacing, and the minimum TTC.

**Table 4**

The comparison between the four models for each AV.

AV ID	Index	Compare with CM		Index	Compare with SM		Index	Compare with CM	
		OM1	OM2		OM1	OM1		OM1	OM2
1	$SD_v$	4.26 %	4.33 %	$\bar{s}$	75.61 %	83.86 %	$\min TTC_i(t)$	163.26 %	171.67 %
2		4.14 %	4.30 %		64.35 %	77.48 %		75.36 %	74.32 %
3		4.52 %	4.64 %		72.38 %	81.76 %		189.28 %	205.31 %
4		2.32 %	2.39 %		64.16 %	76.78 %		92.67 %	93.93 %
Mean		3.81 %	3.92 %		69.13 %	79.97 %		130.14 %	136.31 %

spacing, and minimum TTC are provided in Eqs. (42) to (45), respectively.

$$SD_v = \sqrt{\frac{1}{I} \sum_{i \in \mathcal{I}} \left( \frac{1}{T_i} \sum_{t=t_i}^{t_f} (v_i(t) - \bar{v})^2 \right)} \quad (42)$$

$$\bar{s} = \frac{1}{I} \sum_{i \in \mathcal{I}} \left( \frac{1}{T_i} \sum_{t=t_i}^{t_f} (p_{i-1}(t) - p_i(t)) \right), \forall i \in \mathcal{I} \setminus \{0\} \quad (43)$$

where,

$$\bar{v} = \frac{1}{I} \sum_{i \in \mathcal{I}} \left( \frac{1}{T_i} \sum_{t=t_i}^{t_f} v_i(t) \right) \quad (44)$$

$$\min TTC_i(t) = \min \frac{p_{i-1}(t) - p_i(t) - l}{v_i(t) - v_{i-1}(t)}, \forall v_i(t) > v_{i-1}(t), i \in \mathcal{I} \setminus \{0\} \quad (45)$$

For EQ2, it can be shown that the spacing of the CMs fluctuates around a minimum value of approximately 26 m, while that of the SMs fluctuates around 140 m, peaking at 200 m, as illustrated in Fig. 7. The minimum TTC for CMs fluctuates around a lower value of approximately 10 s, whereas for SMs, it varies near the maximum value of around 30 s. Conversely, the speed SD of the CMs fluctuates around a maximum, while that of the SMs fluctuates around a minimum. These results indicate that the CMs achieve the best mobility at the expense of stability and safety, whereas the SMs prioritize stability and enhanced safety but significantly compromise mobility. The spacing, speed SD, and minimum TTC of OM1s and OM2s lie between those of the CMs and SMs. Specifically, the speed SD of OM1s and OM2s demonstrates an average improvement of approximately 3.8 % and 3.9 %, respectively, compared to that of the CMs, as detailed in Table 4. Furthermore, the average spacing of OM1s and OM2s is reduced by an average of 69.13 % and 79.97 %, respectively, compared to SMs. Additionally, the minimum TTC of OM1s and OM2s increases by an average of 130.14 % and 136.31 %, respectively, compared to the CMs. These findings suggest that the OM1s and OM2s achieve a trade-off between stability and mobility, while maintaining satisfactory performance in safety aspects.

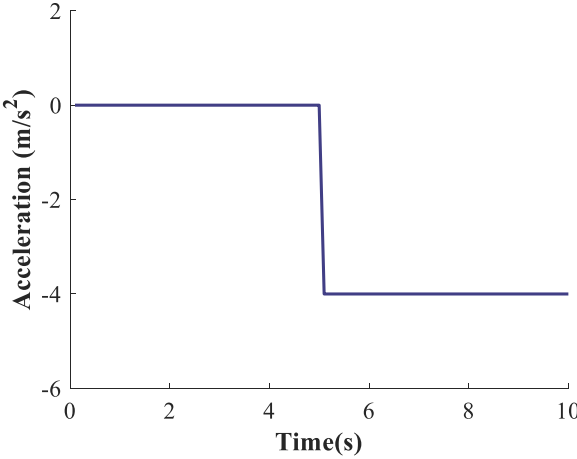
For EQ3, in terms of speed SD, OM1s and OM2s do not exhibit significant differences. However, compared to OM1s, the corresponding spacing of OM2s is reduced by an average of 34.88 %, as detailed in Table 5. Additionally, the minimum TTC of OM2s increases by an average of 2.21 % compared to OM1s. Although the results show that the minimum TTC of AV2 OM1 is slightly higher than that of OM2, the difference is only about 0.1 s. This implies that OM2s significantly improve mobility and safety without compromising stability, compared to OM1s. Notably, stable region 2 is often overlooked in many studies (Sun et al., 2018; Zhou et al., 2019a).

Furthermore, it is important to acknowledge that the data used for calibrating our model inherently represents the smooth-running state of AVs, which constitutes the majority of driving time. Consequently, this approach provides a more generalized perspective on

**Table 5**

The comparison between OM1s and OM2s.

AV ID	$SD_v$	$\bar{s}$	$\min TTC_i(t)$
1	0.08 %	33.82 %	3.20 %
2	0.17 %	36.84 %	-0.59 %
3	0.12 %	33.97 %	5.54 %
4	0.08 %	34.89 %	0.67 %
Mean	0.11 %	34.88 %	2.21 %

**Fig. 8.** Simulation scenario diagram.

AVs, with limited representation of scenarios such as stationary vehicles, red traffic lights, or free-flow states. Therefore, we conducted simulation tests to identify the dynamic range within which our optimal model is applicable. These tests not only clarify the operational boundaries of our model but also offer valuable insights for future efforts in collecting highly dynamic data and developing corresponding models.

We conducted simulations using the optimal CF models for the scenario of cruising followed by braking to a complete stop, diagram as shown in Fig. 8. The optimal model for AV4 was adopted, as shown in Table 4, because the calibration results for AV4's response delay were intermediate (approximately 0.7 s). The simulation involves only two AVs. The simulation terminates if a collision occurs between the AVs; otherwise, it stops when the speed of the following AV reduces to zero. The objective of this simulation is to validate the performance of the proposed models in high-dynamic scenarios. In this study, we define three variables that impact safety metric: cruising speed, braking acceleration, and spacing in the stable CF process, i.e., the preceding and the following vehicle keep the same speed. The cruising speed range was set to [20, 50]m/s, the braking acceleration range was set to [-8, -2] m/s<sup>2</sup>, and the spacing was defined as [20, 80]m. To ensure comprehensive and efficient coverage of the multidimensional parameter space, the low-discrepancy sequences of quasi-random numbers (Montanino et al., 2021) were employed. A total of 2<sup>15</sup> simulations were conducted in this study to achieve robust and reliable results. The minimum TTC is introduced to evaluate the safety of the CF model in various dynamic scenarios, as shown in Eq. (45).

Fig. 9 illustrates the effect of the three variables on the safety of the model. Each point in the figure represents a simulation scenario with a specific combination of cruising speed, braking acceleration, and spacing. The color of each point reflects the safety level of the model in the corresponding scenario (i.e., the minimum TTC). Fig. 9(a) to Fig. 9(c) demonstrate the influence of different spacing and braking accelerations on the safety performance of the model at cruising speeds of 30m/s, 40m/s, and 50m/s, respectively. The results indicate that as the cruising speed increases, the safety of the model progressively deteriorates. Specifically, when the cruising speed exceeds 40m/s, maintaining model safety becomes challenging, as a TTC of <2.5 s is typically considered a dangerous state (Tageldin et al., 2015). A collision occurs when the braking acceleration exceeds -6 m/s<sup>2</sup> and the spacing is less than 60m. When the cruising speed is below 40m/s, model safety can be ensured by maintaining a larger spacing (greater than 60m) combined with moderate braking acceleration (less than -4 m/s<sup>2</sup>). Fig. 9(d) to Fig. 9(f) illustrate the effects of varying spacing and cruising speeds on the safety of the model at braking accelerations of -2 m/s<sup>2</sup>, -4 m/s<sup>2</sup>, and -6 m/s<sup>2</sup>, respectively. The results reveal that when the braking acceleration reaches -6 m/s<sup>2</sup>, the model remains in a dangerous state, even with a larger spacing and a lower cruising speed. As the braking acceleration decreases, the safety of the model gradually improves. When the braking acceleration is lower than -6 m/s<sup>2</sup>, a larger spacing (greater than 60m) and a lower cruising speed (less than 30m/s) can ensure the safety of the model. Fig. 9(g) to Fig. 9(i) illustrate the effects of different braking accelerations and cruising speeds on the safety of the model when the spacing is set to 80m, 50m, and 20m, respectively. The results indicate that when the spacing is reduced to 50m or below, the model remains in a dangerous state even with a lower braking acceleration and cruising speed. When the spacing is 20m, collisions occur across all tested conditions.

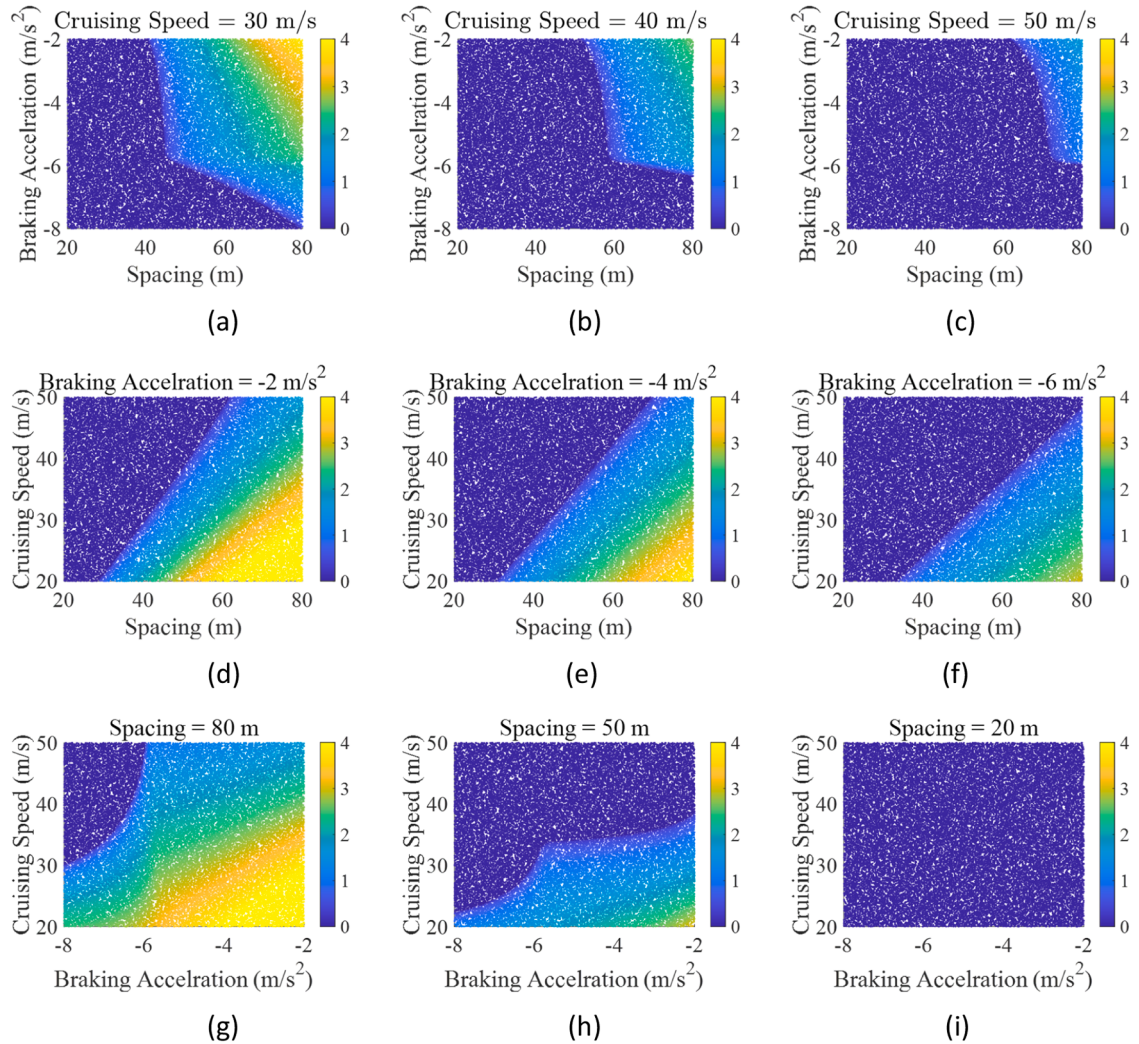


**Fig. 9.** The minimum TTC under different dynamic scenarios based on the OM2 of AV4.

As the spacing increases, the safety of the model shows significant improvement. When the spacing exceeds 50 m, a lower braking acceleration and cruising speed can ensure the model's safety. It is worth noting that the effects of the three variables on the safety of different models follow consistent overall trends but differ on specific threshold values.

Fig. 10 illustrates the safety performance of OM1 for AV4. The results reveal that OM1 exhibits low sensitivity to spacing. This is due to the model's larger time headway, which results in a larger desired spacing. When the braking acceleration exceeds  $-6 m/s^2$ , collisions are observed. When the braking acceleration is below  $-6 m/s^2$ , even under the smallest cruising speed and the largest spacing, the TTC remains around 1 s, indicating a dangerous state. Overall, the OM1 operates dangerously in low-dynamic scenarios and either remains dangerous or results in collisions in high-dynamic scenarios. In comparison, OM2 ensures safety in low-dynamic scenarios. These findings are consistent with the conclusions regarding the safety performance of OM1s and OM2s discussed earlier.

## 6. Conclusion and future work

This paper proposes a general modeling methodology achieving a trade-off between stability and mobility for the linear CF model, while maintaining satisfactory performance in safety aspects. Firstly, a general linear CF model is calibrated, and the response delay of the CF model is identified for 20 AVs in the ULTRA-AV dataset. Next, inequality constraints ensuring both local and string stability of the CF model are derived. An objective function aimed at maximizing mobility is formulated subject to stability constraints, and the optimal model parameters are determined by the GA. The performance of the CM, SM, OM1, and OM2 is compared using speed SD, average spacing, and the minimum TTC as metrics for stability, mobility, and safety, respectively. Finally, the dynamic range of the optimal models is provided. The major insights of the study include:

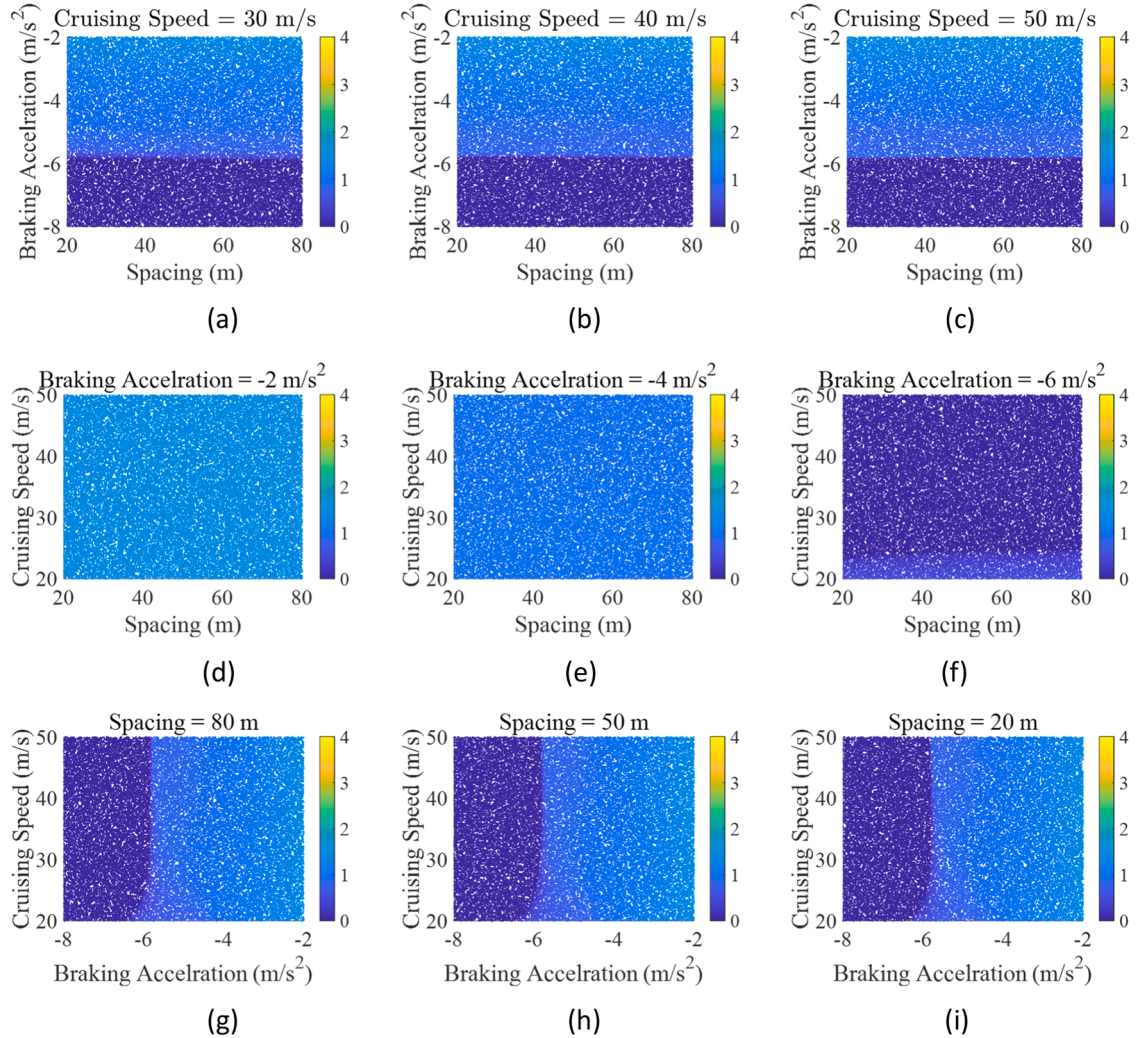


**Fig. 10.** The minimum TTC under different dynamic scenarios based on the OM1 of AV4.

- The response delay of the linear CF model for the 20 commercial AVs is distributed between 0.4 s and 1.1 s, and the CMs for all of the commercial AVs are unstable.
- The OM1s and OM2s achieve a trade-off between stability and mobility, while maintaining satisfactory performance in safety aspects. Compared to OM1s, OM2s demonstrate superior mobility and enhanced safety without compromising stability (and exhibit improved stability in some cases). It is important to emphasize that the superior models in stable region 2, i.e., OM2s, are typically overlooked in most studies.
- The OM2s can ensure safety provided that the initial speed is below 40  $m/s$ , the braking acceleration is less than  $-6 \text{ m/s}^2$ , and the initial spacing exceed 50 m. It is important to note that this conclusion is derived from a specific scenario of rapid deceleration and the particular case of AV4, meaning that the thresholds may vary for different scenarios and models.
- The framework proposed in this paper is fully applicable to third-order dynamic systems.

Overall, this paper proposes a modeling methodology to identify the optimal CF model, ensuring mobility and safety under stability constraints. However, this study has certain limitations, necessitating further research in several key areas:

- The precise boundaries of stable regions need to be further derived. Currently, most studies rely on approximate derivations of stable regions, which inevitably limits the accuracy of identifying optimal models.
- Further on-road tests involving commercial AVs should be conducted to validate the dynamic range of the proposed methodology. Although this study is based on empirical data, it incorporates several assumptions, such as neglecting parasitic lag and assuming a homogeneous platoon, which may not fully reflect real-world conditions.

## CRediT authorship contribution statement

**Yuqin Zhang:** Visualization, Methodology, Writing – original draft, Formal analysis, Software. **Ke Ma:** Formal analysis, Writing – review & editing, Data curation, Methodology, Conceptualization. **Zhigang Xu:** Supervision, Writing – review & editing, Conceptualization. **Hang Zhou:** Data curation, Software. **Chengyuan Ma:** Software, Writing – review & editing. **Xiaopeng Li:** Conceptualization, Writing – review & editing, Supervision, Methodology.

## Acknowledgments

Yuqin Zhang was supported by the Fundamental Research Funds for the Central Universities, CHD, under grant 300102243713. All other authors were not supported by any funding.

## Appendix

**Table A.1**

The calibration results for 20 AVs in ULTRA-AV dataset.

Data	Vehicle ID	$f_i^{\Delta v} (s^{-1})$	$f_i^{\Delta p} (s^{-2})$	$f_i^v (s^{-1})$	$z_i (m/s^2)$	$\theta_i (s)$	Stability
ZalaZone	1	0.3659	0.0328	-0.0241	-0.2343	0.6	Unstable
	2	0.5250	0.1356	-0.1375	-0.4999	0.6	Unstable
	3	0.3622	0.0293	-0.0160	-0.4999	1.1	Unstable
	4	0.3427	0.1095	-0.1738	-0.3798	0.5	Unstable
	5	0.2805	0.0558	-0.1469	-0.1430	1.0	Unstable
	6	0.2771	0.0958	-0.1948	-0.3465	0.9	Unstable
	7	0.2256	0.0538	-0.1005	-0.4975	0.8	Unstable
	8	0.6972	0.0412	-0.0187	-0.4998	0.8	Unstable
	9	0.7053	0.0854	-0.0637	-0.4771	0.6	Unstable
	10	0.2794	0.1144	-0.1997	-0.2038	0.5	Unstable
Casale	1	0.2308	0.0714	-0.0807	-0.4655	0.7	Unstable
	1	0.3091	0.0876	-0.0984	-0.1865	0.4	Unstable
	2	0.1666	0.0684	-0.1622	-0.1618	1.0	Unstable
	3	0.346	0.0751	-0.0775	-0.2091	0.5	Unstable
CATS	4	0.4225	0.1757	-0.1814	-0.5	0.7	Unstable
	1	0.0167	0.0930	-0.1486	-0.4104	0.7	Unstable
	2	0.2573	0.0158	-0.0069	-0.4225	0.5	Unstable
Ohio	1	0.1056	0.0516	-0.1243	-0.1833	0.7	Unstable
	2	0.1866	0.0107	-0.0206	-0.1488	0.8	Unstable
	3	0.0771	0.0580	-0.0697	-0.2052	0.6	Unstable

**Table A.2**

The optimal parameters for the calibrated response delay.

(s)	$f_i^{\Delta v} (s^{-1})$	$f_i^{\Delta p} (s^{-2})$	$f_i^v (s^{-1})$	Stable Region
0.4	0.0010	1.0333	-1.4461	Stable Region 1
0.5	0.0010	0.6633	-1.1633	
0.6	0.0010	0.4545	-0.9686	
0.7	0.0010	0.3455	-0.8324	
0.8	0.0010	0.2584	-0.7207	
0.9	0.0010	0.2057	-0.6450	
1.0	0.0010	0.1662	-0.5795	
1.1	0.0010	0.1398	-0.5301	
0.4	1.2296	0.0548	-0.0442	Stable Region 2
0.5	0.9767	0.0589	-0.0604	
0.6	0.8153	0.0277	-0.0335	
0.7	0.6863	0.0367	-0.0522	
0.8	0.5989	0.0298	-0.0485	
0.9	0.4817	0.0956	-0.1894	
1.0	0.4667	0.0346	-0.0715	
1.1	0.4063	0.0468	-0.1101	

## References

- Bareket, Z., Fancher, P.S., Huei, P., Kangwon, L., Assaf, C.A., 2003. Methodology for assessing adaptive cruise control behavior. IEEE Trans. Intell. Transp. Syst. 4, 123–131. <https://doi.org/10.1109/TITS.2003.821288>.

- Chandler, R.E., Herman, R., Montroll, E.W., 1958. Traffic dynamics: studies in car following. *Oper. Res.* 6, 165–184. <https://doi.org/10.1287/opre.6.2.165>.
- Chen, D., Laval, J., Zheng, Z., Ahn, S., 2012. A behavioral car-following model that captures traffic oscillations. *Transp. Res. Part B Methodol.* 46, 744–761. <https://doi.org/10.1016/j.trb.2012.01.009>.
- Davis, L.C., 2004. Effect of adaptive cruise control systems on traffic flow. *Phys. Rev. E* 69, 066110. <https://doi.org/10.1103/PhysRevE.69.066110>.
- Feng, S., Zhang, Y., Li, S.E., Cao, Z., Liu, H.X., Li, L., 2019. String stability for vehicular platoon control: definitions and analysis methods. *Annu. Rev. Control* 47, 81–97. <https://doi.org/10.1016/j.arcontrol.2019.03.001>.
- Gunter, G., Gloudemans, D., Stern, R.E., McQuade, S., Bhadani, R., Bunting, M., Delle Monache, M.L., Lysecky, R., Seibold, B., Sprinkle, J., Piccoli, B., Work, D.B., 2021. Are commercially implemented adaptive cruise control systems string stable? *IEEE Trans. Intell. Transp. Syst.* 22, 6992–7003. <https://doi.org/10.1109/TITS.2020.3000682>.
- Gunter, G., Janssen, C., Barbour, W., Stern, R.E., Work, D.B., 2020. Model-based string stability of adaptive cruise control systems using field data. *IEEE Trans. Intell. Veh.* 5, 90–99. <https://doi.org/10.1109/TIV.2019.2955368>.
- Hung, N.V., Luu, D.L., Dong, N.S., Lupu, C., 2024. Reducing time headway for cooperative vehicle following in platoon via information flow topology. *J. Control Eng. Appl. Inform.* 26, 77–87. <https://doi.org/10.61416/ceai.v26i2.8834>.
- Jiang, J., Zhou, Y., Jafarsalehi, G., Wang, X., Ahn, S., Lee, J.D., 2025. Stochastic calibration of automated vehicle car-following control: an approximate Bayesian computation approach. *IEEE Trans. Intell. Transp. Syst.* 26, 3115–3127. <https://doi.org/10.1109/TITS.2025.3526318>.
- Jiang, R., Jin, C.-J., Zhang, H.M., Huang, Y.-X., Tian, J.-F., Wang, W., Hu, M.-B., Wang, H., Jia, B., 2017. Experimental and empirical investigations of traffic flow instability. *Transp. Res. Procedia* 23, 157–173. <https://doi.org/10.1016/j.trpro.2017.05.010>.
- Laval, J.A., Leclercq, L., 2010. A mechanism to describe the formation and propagation of stop-and-go waves in congested freeway traffic. *Philos. Trans. R. Soc. Math. Phys. Eng. Sci.* 368, 4519–4541. <https://doi.org/10.1098/rsta.2010.0138>.
- Li, D., Wagner, P., 2019. Impacts of gradual automated vehicle penetration on motorway operation: a comprehensive evaluation. *Eur. Transp. Res. Rev.* 11, 36. <https://doi.org/10.1186/s12544-019-0375-3>.
- Li, X., 2022. Trade-off between safety, mobility and stability in automated vehicle following control: an analytical method. *Transp. Res. Part B Methodol.* 166, 1–18. <https://doi.org/10.1016/j.trb.2022.09.003>.
- Ma, K., Li, X., 2022. Empirical study of feedback delay in stability analysis for production vehicles with different powertrains. In: Proceeding of the IEEE 25th International Conference on Intelligent Transportation Systems (ITSC). Macau, China. IEEE, pp. 4196–4201. <https://doi.org/10.1109/ITSC55140.2022.9922215>. Presented at the 2022 IEEE 25th International Conference on Intelligent Transportation Systems (ITSC).
- Ma, K., Wang, H., Zuo, Z., Hou, Y., Li, X., Jiang, R., 2022. String stability of automated vehicles based on experimental analysis of feedback delay and parasitic lag. *Transp. Res. Part C Emerg. Technol.* 145, 103927. <https://doi.org/10.1016/j.trc.2022.103927>.
- Ma, K., Zhou, H., Liang, Z., Li, X., 2025. Automated vehicle microscopic energy consumption study (AV-Micro): data collection and model development. *Energy* 320, 135096. <https://doi.org/10.1016/j.energy.2025.135096>.
- Milanés, V., Shladover, S.E., 2014. Modeling cooperative and autonomous adaptive cruise control dynamic responses using experimental data. *Transp. Res. Part C Emerg. Technol.* 48, 285–300. <https://doi.org/10.1016/j.trc.2014.09.001>.
- Montanino, M., Monteil, J., Punzo, V., 2021. From homogeneous to heterogeneous traffic flows: Lp string stability under uncertain model parameters. *Transp. Res. Part B Methodol.* 146, 136–154. <https://doi.org/10.1016/j.trb.2021.01.009>.
- Punzo, V., Zheng, Z., Montanino, M., 2021. About calibration of car-following dynamics of automated and human-driven vehicles: methodology, guidelines and codes. *Transp. Res. Part C Emerg. Technol.* 128, 103165. <https://doi.org/10.1016/j.trc.2021.103165>.
- Robert, H., Elliott, W.M., Renfrey, B.P., Richard, W.R., 1959. Traffic dynamics: analysis of stability in car following. *Oper. Res.* 7, 86–106.
- Shi, X., Li, X., 2021. Empirical study on car-following characteristics of commercial automated vehicles with different headway settings. *Transp. Res. Part C Emerg. Technol.* 128, 103134. <https://doi.org/10.1016/j.trc.2021.103134>.
- Stern, R.E., Cui, S., Delle Monache, M.L., Bhadani, R., Bunting, M., Churchill, M., Hamilton, N., Haulcy, R., Pohlmann, H., Wu, F., Piccoli, B., Seibold, B., Sprinkle, J., Work, D.B., 2018. Dissipation of stop-and-go waves via control of autonomous vehicles: field experiments. *Transp. Res. Part C Emerg. Technol.* 89, 205–221. <https://doi.org/10.1016/j.trc.2018.02.005>.
- Sun, J., Zheng, Z., Sun, J., 2020. The relationship between car following string instability and traffic oscillations in finite-sized platoons and its use in easing congestion via connected and automated vehicles with IDM based controller. *Transp. Res. Part B Methodol.* 142, 58–83. <https://doi.org/10.1016/j.trb.2020.10.004>.
- Sun, J., Zheng, Z., Sun, J., 2018. Stability analysis methods and their applicability to car-following models in conventional and connected environments. *Transp. Res. Part B Methodol.* 109, 212–237. <https://doi.org/10.1016/j.trb.2018.01.013>.
- Swaroop, D., Rajagopal, K.R., 2001. A review of constant headway policy for automatic vehicle following. In: Proceedings of the ITSC 2001. 2001 IEEE Intelligent Transportation Systems, pp. 65–69. <https://doi.org/10.1109/ITSC.2001.948631>. Proceedings (Cat. No.01TH8585). Presented at the ITSC 2001. 2001 IEEE Intelligent Transportation Systems. Proceedings (Cat. No.01TH8585).
- Tadaki, S., Kikuchi, M., Fukui, M., Nakayama, A., Nishinari, K., Shibata, A., Sugiyama, Y., Yosida, T., Yukawa, S., 2013. Phase transition in traffic jam experiment on a circuit. *New J. Phys.* 15, 103034. <https://doi.org/10.1088/1367-2630/15/10/103034>.
- Tageldin, A., Sayed, T., Shaaban, K., Zaki, M.H., 2015. Automated analysis and validation of right-turn merging behavior. *J. Transp. Saf. Secur.* 7, 138–152. <https://doi.org/10.1080/19439962.2014.942019>.
- Tian, B., Wang, G., Xu, Z., Zhang, Y., Zhao, X., 2021. Communication delay compensation for string stability of CACC system using LSTM prediction. *Veh. Commun.* 29, 100333. <https://doi.org/10.1016/j.vehcom.2021.100333>.
- Treibel, M., Helbing, D., 2001. Microsimulations of freeway traffic including control measures. *Auto* 49, 478. <https://doi.org/10.1524/auto.2001.49.11.478>.
- Treibel, M., Kesting, A., 2013. Traffic Flow Dynamics: Data, Models and Simulation. Springer, Berlin, Heidelberg. <https://doi.org/10.1007/978-3-642-32460-4>.
- Wang, J., Zhou, A., Liu, Z., Peeta, S., 2024. Robust cooperative control strategy for a platoon of connected and autonomous vehicles against sensor errors and control errors simultaneously in a real-world driving environment. *Transp. Res. Part B Methodol.* 184, 102946. <https://doi.org/10.1016/j.trb.2024.102946>.
- Wang, X., Liu, Q., Guo, F., Fang, S., Xu, X., Chen, X., 2022. Causation analysis of crashes and near crashes using naturalistic driving data. *Accid. Anal. Prev.* 177, 106821. <https://doi.org/10.1016/j.aap.2022.106821>.
- Zhang, Y., Tian, B., Xu, Z., Gong, S., Gao, Y., Cui, Z., Chen, X., 2022. A local traffic characteristic based dynamic gains tuning algorithm for cooperative adaptive cruise control considering wireless communication delay. *Transp. Res. Part C Emerg. Technol.* 142, 103766. <https://doi.org/10.1016/j.trc.2022.103766>.
- Zhang, Y., Xu, Z., Wang, Z., Yao, X., Xu, Z., 2023. Impacts of communication delay on vehicle platoon string stability and its compensation strategy: a review. *J. Traffic Transp. Eng. Engl. Ed.* 10, 508–529.
- Zhong, X., Zhou, Y., Kamaraj, A.V., Zhou, Z., Kontar, W., Negrusi, D., Lee, J.D., Ahn, S., 2025. Human-automated vehicle interactions: voluntary driver intervention in car-following. *Transp. Res. Part C Emerg. Technol.* 171, 104969. <https://doi.org/10.1016/j.trc.2024.104969>.
- Zhou, H., Ma, K., Liang, S., Li, X., Qu, X., 2024. ULTRA-AV: a unified longitudinal trajectory dataset for automated vehicle. Presented at. In: Proceedings of the IEEE Intelligent Vehicles Symposium (IV).
- Zhou, Y., Ahn, S., Wang, M., Hoogendoorn, S., 2019a. Stabilizing mixed vehicular platoons with connected automated vehicles: an H-infinity approach. *Transp. Res. Procedia* 38, 441–461. <https://doi.org/10.1016/j.trpro.2019.05.024>.
- Zhou, Y., Wang, M., Ahn, S., 2019b. Distributed model predictive control approach for cooperative car-following with guaranteed local and string stability. *Transp. Res. Part B Methodol.* 128, 69–86. <https://doi.org/10.1016/j.trb.2019.07.001>.
- Zhou, Y., Zhong, X., Chen, Q., Ahn, S., Jiang, J., Jafarsalehi, G., 2023. Data-driven analysis for disturbance amplification in car-following behavior of automated vehicles. *Transp. Res. Part B Methodol.* 174, 102768. <https://doi.org/10.1016/j.trb.2023.05.005>.